Communication

An Experimental-Based Analysis of Inter-BAN Co-Channel Interference Using the κ-μ Fading Model

Nidhi Bhargav, Simon L. Cotton, and David B. Smith

***Abstract*— In this communication, we empirically study and model the impact of co-channel interference and background noise (BN) on a body area network (BAN) operating at 2.48 GHz using the extremely generalized κ-μ fading model. The BAN measurements considered three nodes with the signal-of-interest (SoI) forming the link between two wearable devices located on the front-central-chest and front-central-waist of an adult male, while an interfering signal emanated from a third wearable device that was located on the front-central-waist of an adult female. Three environments were considered which are indicative of different environmental multipath conditions likely to be encountered by everyday BAN users, namely, an anechoic chamber, a reverberation chamber and an indoor laboratory. As well as this, the influence of different human mobility scenarios was studied. Utilizing the κ and μ parameter estimates, we then provide some useful insights into the outage performance of BAN systems in the presence of BN when both the SoI and the interferer undergo κ-μ fading.**

***Index Terms*— κ-μ fading, body area networks (BANs), co-channel interference (CCI), on-body propagation.**

I. Introduction

Body area networks (BANs) encompass groupings of wearable and implantable sensors that are placed in, on, around or in close proximity to the human body. These networks have drawn a lot of attention for their use in healthcare, sports, military, and consumer applications. As a consequence of the increasing proliferation of BAN technology, they are becoming more susceptible to interference from nearby BANs and wireless networks, which may degrade the quality of BAN links. Quite often, the first step in modeling the potential impact of co-channel interference (CCI) in BANs is a thorough characterization of the propagation channels responsible for carrying the signal-of-interest (SoI) and the interfering signal. To this end, several studies have been conducted which have investigated fading in on-body channels [1]–[4]. For example, in [3], the effect of user states in different environmental multipath conditions was investigated and the short-term fading component characterized using the Nakagami-*m*, Rice and lognormal fading models. Similarly, several studies have investigated fading in body-to-body (B2B) channels [5]–[9]. Notably, [5], [6] successfully used the κ-μ fading model [10] to statistically describe the short-term fading observed in dynamic B2B channels whilst [8] used the gamma distribution to describe amplitude fading for various body movements in an indoor area at 2.45 and 5.8 GHz.

Manuscript received May 21, 2016; revised October 25, 2016; accepted November 9, 2016. Date of publication December 15, 2016; date of current version February 1, 2017. This work was supported by the U.K. Engineering and Physical Sciences Research Council under Grant Reference EP/L026074/1.

N. Bhargav and S. L. Cotton are with the Wireless Communications Laboratory, Institute of Electronics, Communications, and Information Technology, The Queen's University of Belfast, Belfast BT3 9DT, U.K. (e-mail: nbhargav01@qub.ac.uk; simon.cotton@qub.ac.uk).

D. B. Smith is with Data61 CSIRO, Eveleigh, NSW 2015, Australia, and also with Australian National University, Canberra, ACT 0200, Australia (e-mail: david.smith@data61.csiro.au).

Color versions of one or more of the figures in this communication are available online at http://ieeexplore.ieee.org.

Digital Object Identifier 10.1109/TAP.2016.2634521

Although several studies have reported the impact of CCI and interference caused by nearby networks on BANs [11]–[15], physical layer research on interference in BANs is relatively limited. Most notably, interference measurements for BANs operating at 2.45 GHz were conducted in [11]. It was reported that the worst-case interference in a given BAN is expected to be caused by other BANs residing in the local vicinity. The interuser interference between co-located BAN users undertaking a variety of body movements in an indoor environment was experimentally investigated at 2.45 and 60 GHz in [12]. Specifically, the carrier-to-interference ratio and the interference power-level variations were characterized. Critically, both [12] and [13] have shown that this type of interference is significant and needs to be addressed, if BANs are to be extensively and successfully deployed in the future. Moreover, [13] and [14] propose using fixed network infrastructure and diversity techniques to mitigate interference.

Despite the aforementioned research on the impact of CCI on BANs, to the best of the authors' knowledge none of the previous studies have performed a systematic investigation of the performance of BAN channels which undergo κ-μ fading in the presence of CCI and background noise (BN). In this contribution, we first focus on performing some inter-BAN interference measurements at 2.48 GHz using antennas designed specifically for BAN applications. Following from this, we provide a novel statistical characterization of the on-body SoI and the inter-BAN interfering channels at 2.48 GHz using the κ-μ fading model. We then provide some insights into the outage performance of BANs in the presence of BN when the SoI and the interferer are subject to κ-μ fading which will be beneficial for the future design of BAN systems.

The remainder of this communication is organized as follows. Section II explains the measurement procedure, interference scenarios and data analysis. Section III provides a characterization of the short-term fading in BAN and inter-BAN channels. An experimental analysis of the outage performance of BANs in the presence of CCI and BN is presented in Section IV. Lastly, Section V finishes this communication with some concluding remarks.

II. Interference Measurements and Analysis

A. Measurement Setup and Environments

The measurements performed in this study were conducted in the ECIT building at Queen's University Belfast in the United Kingdom. As shown in Fig. 1, three separate measurement environments located on the ground floor of the ECIT building, namely, an anechoic chamber (54 m^2), a reverberation chamber (5.8 m^2) and an indoor laboratory (46.11 m^2) were chosen. The ECIT building mainly consists of metal studded dry walls with metal tiled floors covered with polypropylene-fiber, rubber backed carpet tiles, a metal ceiling with mineral fiber tiles and recessed louvered luminaries suspended 2.7 m above floor level. The anechoic chamber is housed in conductive shielding and lined with pyramidal RF absorbers whilst the reverberation chamber is constructed entirely from metal and

This work is licensed under a Creative Commons Attribution 3.0 License. For more information, see http://creativecommons.org/licenses/by/3.0/

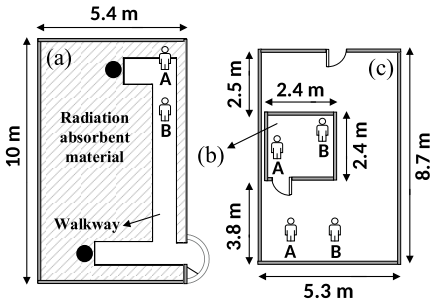

Fig. 1. Plan view of the (a) anechoic chamber, (b) reverberation chamber, and (c) laboratory environment. A and B denote the positions of the test subject's in each of the measurement environments. Solid circles represent nonconducting support structures in the anechoic chamber.

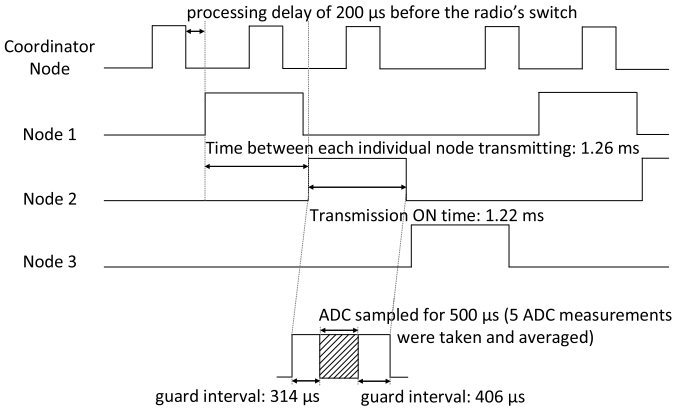

Fig. 2. Timing diagram showing the operation of the measurement system.

is equipped with two mechanical plate stirrers, polarization stirring and platform stirring. The indoor laboratory area contained some chairs, several desks constructed from medium density fiberboard, a white board, and a PC. These environments are considered to be illustrative of the minimum (anechoic), extreme (reverberation) and typical (laboratory) environmental multipath conditions likely to be experienced by everyday BAN users.[1]

Each hypothetical BAN node consisted of two transceiver boards, a measurement radio board and a controller radio board. The measurement radio was an ML2730, manufactured by RFMD, which was configured to operate at 2.48 GHz. When acting as a transmitter, the hypothetical BAN nodes transmitted a continuous wave signal with an output power level of +17.6 dBm. Conversely, when functioning as a receiver, these nodes recorded the received signal strength (RSS) using a 12-bit analogue-to-digital convertor (ADC) of the attached controller radio. The controller radio was a CC1110F32 manufactured by Texas Instruments and operated at 868 MHz. The purpose of the controller radio was to synchronize the operation of the hypothetical BAN nodes. As well as this, it determined whether the measurement radio operated as a transmitter or a receiver according to a time-slotted, round robin protocol. A central coordinator broadcasted a packet to all of the controller radios to signify the current timeslot. To make the system more robust, each controller had a timer that was updated upon receiving a coordinator packet, and automatically switched states if a coordinator packet was not received. Additionally, all information broadcasted by the controller radio on each node and the coordinator was centrally recorded by a base-station connected to a PC.

[1]To facilitate a study of the envelope variation solely due to body movements, the mechanical stirrers in the reverberation chamber were disabled.

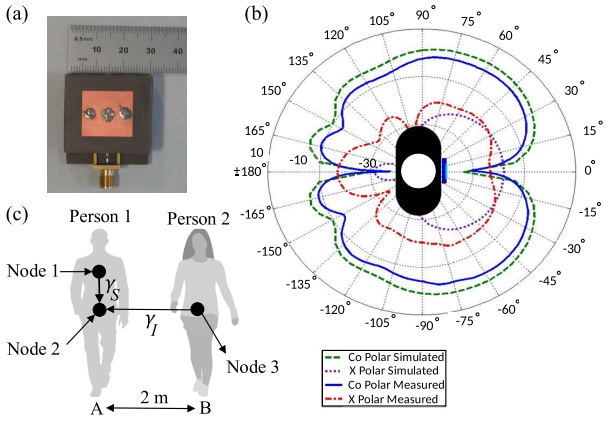

Fig. 3. (a) HMMPA. (b) Simulated far-field radiation patterns of HMMPA in azimuth plane at 2.484 GHz when placed on a human tissue phantom. (c) Position of BAN nodes. On-body transmitter located on front-chest of person 1 (Node 1) and front-central-waist of person 2 (Node 3). Receiver positioned on the front-central-waist of person 1 (Node 2). SoI operated between Nodes 1 and 2, while the interfering signal operated between Nodes 3 and 2. A and B denote the positions of the test subjects in each of the environments.

The operation of the channel measurement system is illustrated using the timing diagram shown in Fig. 2. During any particular time-slot, only one node could operate as a transmitter while the others acted as receivers and sampled the RSS. When acting as the transmitter, each node was on for 1.22 ms, while the receivers sampled the channels for 500 μs (5 ADC measurements were taken and averaged). To ensure that the RF circuitry within the measurement radios had sufficient time to settle and to allow the RSS output to become stable, guard intervals were added before and after each RSS measurement window. The time between each individual node transmitting was 1.26 ms, which for a three node system meant that one super-frame was transmitted every 5.04 ms, i.e., $(N + 1) \times 1.26$ ms, where N represents the number of nodes (equal to the number of time-slots). It is important to note that an extra time-slot was added to each super-frame to allow all of the controller radios to be recalibrated.

As shown in Fig. 3(a), the antennas used in this study were compact (5.75 mm height and a patch element size of 22 × 22 mm) higher mode microstrip patch antennas (HMMPAs) which operate within the Industrial Scientific and Medical (ISM) frequency allocation of 2.401–2.484 GHz. Fig. 3(b) shows that the HMMPA has a monopole type radiation pattern when mounted normal to the body surface. It is worth highlighting that this antenna was specifically designed for efficient BAN communications [16]. In the experiments conducted here, the HMMPAs were mounted on a 5 mm Rohacell HF51 foam dielectric spacer ($\epsilon_r = 1.07$), to maintain consistent antenna-body separation distance.

B. Inter-BAN Interference

To characterize the potential interference between co-located BANs, two persons were fitted with a number of hypothetical BAN nodes as shown in Fig. 3(c). In this example usage scenario, a node placed on the front-central-chest (Node 1) of person 1 sends a signal to a master node located on the front-central-waist (Node 2) of the same person. A third node (Node 3) located on the front-central-waist of another person transmits an interfering signal that has the potential to corrupt the data being received by the master node.

For this study, the SoI operated between Nodes 1 and 2, whilst the interfering signal existed between Nodes 3 and 2. The test subjects,

namely, person 1 and person 2 were an adult male and a female of height 1.83 and 1.65 m, mass 80 and 53 kg, respectively. The study was further extended to include two user state scenarios in each of the environments. The users were initially instructed to stand motionless at positions A and B, separated by a distance of 2 m. In scenario 1, person 2 who was located at position B was instructed to move around randomly within a circle of radius 0.5 m from their starting position whilst person 1 remained stationary. Scenario 2 involved both users exhibiting random movements within a circle of radius 0.5 m from their starting positions.

C. Data Analysis

One focus of this study is to provide a statistical characterization of the short-term fading for dynamic BAN scenarios operating in different environmental multipath conditions. To this end, we use a generalized fading model, namely the κ-μ fading model which has been previously used to successfully characterize the envelope fading in body-centric communications [5], [6]. The probability density function (pdf) of the κ-μ fading signal envelope, R, is given in [10, eq. 11] whilst the pdf of the instantaneous signal-to-noise-ratio (SNR), γ, of a κ-μ fading channel is obtained from the envelope pdf via a transformation of variables $\left(r = \sqrt{\gamma\ \bar{r}^2/\bar{\gamma}}\right)$ as

$$f_\gamma(\gamma) = \frac{\mu(1+\kappa)^{\frac{\mu+1}{2}}\gamma^{\frac{\mu-1}{2}}e^{\frac{-\mu(1+\kappa)\gamma}{\bar{\gamma}}}}{\kappa^{\frac{\mu-1}{2}}\bar{\gamma}^{\frac{\mu+1}{2}}e^{\mu\kappa}} I_{\mu-1}\left(2\mu\sqrt{\frac{\kappa(1+\kappa)\gamma}{\bar{\gamma}}}\right) \tag{1}$$

where $\bar{r}$ is the root-mean square value of R, $\kappa > 0$ is the ratio of the total power of the dominant components to that of the scattered waves, $\mu > 0$ is related to the number of multipath clusters, $I_n(\cdot)$ is the modified Bessel function of the first kind and order n, and $\bar{\gamma} = \mathbb{E}(\gamma)$ is the average SNR. It is worth highlighting that the κ-μ fading model contains many popular fading models as special cases, such as the Rice ($\mu = 1$; $\kappa = K$), Nakagami-m ($\mu = m$; $\kappa \to 0$), Rayleigh ($\mu = 1$; $\kappa \to 0$), and One-Sided Gaussian ($\mu = 0.5$; $\kappa \to 0$).

For the analysis conducted here, the sampled RSS data were imported into MATLAB and the data sets were normalized to their respective local means. To do this, the raw data were visually examined and overlaid with the local mean signal for differing window sizes. An appropriate smoothing window of 75 samples was then chosen for all of the experiments. The parameter estimates were obtained using the κ-μ pdf given in [10, eq. 11] and the `lsqnonlin` function, available in the optimization toolbox of MATLAB. A cumulative total of 45 000 samples were collected with a maximum average noise floor level of -103.4 dBm, whilst the lowest recorded sample during testing was -100.1 dBm.

In order to ensure that the short-term fading measurements conducted in this study were collected within the coherence time of the channel, we performed a separate set of measurements for all of the environments and scenarios. These were performed for each link individually, for a duration of 10 s using a sample frequency of 10 kHz. In [17], the coherence time is defined as the time over which the time correlation function is above 0.5. For this level, the lowest coherence time was found to be 68.2 ms. Therefore, considering the worst case scenario we were able to sample at least 13 times within the coherence time of the channel.[2]

[2]Increasing the time correlation levels to 0.7 and 0.95, the lowest coherence times were found to be 47.5 and 17.2 ms, respectively, meaning that from a practical point of view the measurements of the SoI and interferer's channels can be considered as being simultaneous.

TABLE I

PARAMETER ESTIMATES FOR THE κ-μ FADING MODEL FITTED TO THE MEASURED DATA OBTAINED FROM THE ANECHOIC CHAMBER, REVERBERATION CHAMBER, AND INDOOR LABORATORY*

Multipath environment	Scenarios	$\hat{\kappa}_S$	$\hat{\mu}_S$	$\hat{\kappa}_I$	$\hat{\mu}_I$
Anechoic chamber	Scenario 1	60.0	0.47	34.1	0.35
	Scenario 2	63.3	0.49	41.7	0.15
Reverberation chamber	Scenario 1	19.8	0.69	7.09	0.51
	Scenario 2	5.70	0.63	2.91	0.72
Laboratory environment	Scenario 1	29.9	1.05	6.80	0.81
	Scenario 2	11.8	0.94	4.80	0.72

*It should be noted that $\hat{\bar{r}}_S$ and $\hat{\bar{r}}_I$ were close to unity for all scenarios.

III. BAN/INTER-BAN CHANNEL CHARACTERIZATION

In this section, using the approach described in Section II, we fit the envelope pdf of the κ-μ fading model to the empirical densities obtained for all of the measured channels. To allow the reader to reproduce the plots obtained here, Table I provides a summary of the parameter estimates obtained for all measurement environments and scenarios. It should be noted that $\{\kappa_S, \mu_S, \bar{r}_S\}$ and $\{\kappa_I, \mu_I, \bar{r}_I\}$ represent the channel components of the SoI and the interfering signals, respectively.

A. Anechoic Chamber

Fig. 4(a) shows the excellent fit that the pdf of the κ-μ fading model provides to the empirical data for both the on-body and inter-BAN channels for scenario 1. From Table I, it is immediately obvious that the parameter estimates for κ_S and κ_I are large indicating that these channels are strongly influenced by dominant signal components. As well as this, it can be seen that the estimate of κ for the SoI was greater than that of the interfering channel. A possible explanation for this observation is the fact that the antennas used here were specifically designed for on-body communications and therefore maximized gain in the on-body direction while presenting a null in the off-body direction. As a result, the dominant signal components arriving from the direction of the interferer would have experienced a reduced gain resulting in a lower κ value. It is also seen that the parameter estimate of μ for the SoI is greater than that observed for the interfering channel. This indicates that there is a greater fading severity for the interfering link when compared to the SoI.

For scenario 2, the κ-μ pdf provides a very good approximation to the channel measurements obtained for the SoI and the interfering links [Fig. 4(b)]. Despite both persons now moving randomly, high κ estimates are again obtained for both the on-body and the inter-BAN channels while the estimate of κ for the interfering channel is significantly greater than that observed for the SoI. Similar to scenario 1, low values of μ estimates were seen for both the SoI and the interfering links presumably as a result of the minimal environmental multipath contributions offered by the anechoic surroundings.

B. Reverberation Chamber

Fig. 4(c) and (d) shows the empirical pdf of the on-body and the inter-BAN channels for scenarios 1 and 2 in the reverberation chamber alongside the κ-μ distribution. As mentioned in Section II, the mechanical stirrers in the reverberation chamber were disabled in order to facilitate a study of the envelope signal variation solely due to body movements. Therefore, the chamber now represents

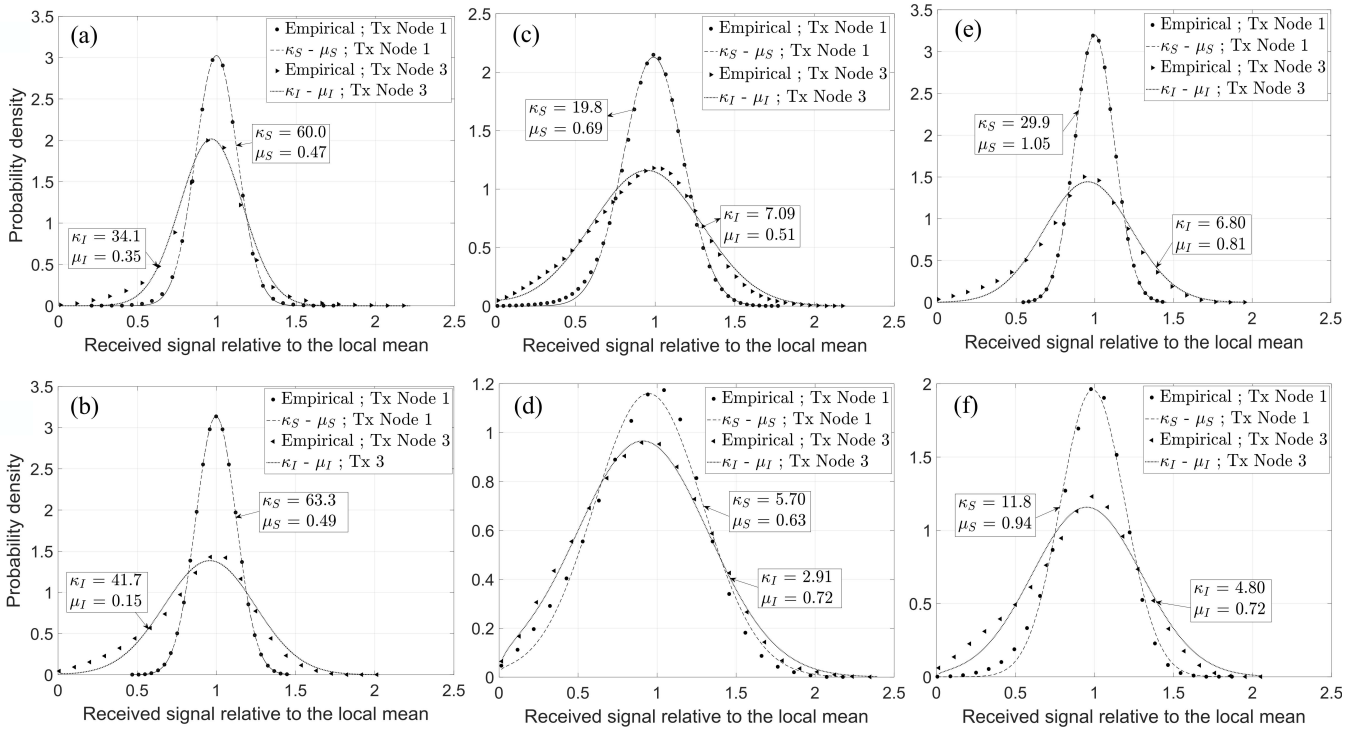

Fig. 4. Empirical envelope pdf of the SoI and interfering links for (a) anechoic chamber scenario 1, (b) anechoic chamber scenario 2, (c) reverberation chamber scenario 1, (d) reverberation chamber scenario 2, (e) laboratory environment scenario 1, and (f) laboratory environment scenario 2 compared to the κ-μ pdf.

a highly reflective environment with a finite number of multipath components. This is illustrated by the low estimates of μ observed for the SoI and the interfering channels which were obtained for both scenarios 1 and 2 (Table I). Compared to the anechoic chamber, the estimated κ parameters for both the SoI and interfering channels (although relatively large) were significantly reduced, with scenario 2 experiencing the lowest κ estimates.

C. Laboratory Environment

From Fig. 4(e) and (f), we observe that the κ-μ distribution again provides an excellent fit to the empirical densities of the on-body and inter-BAN data for both scenarios in the laboratory environment. Inspecting Table I, with the exception of the interfering link during scenario 2, the estimated κ parameters are greater than those obtained for the reverberation chamber. Identical to all of the other environments, we again see that κ_S is greater than κ_I, and μ_S is greater than μ_I for both scenarios. Furthermore, as the indoor laboratory offered a richer scattering environment, the estimates of μ_S and μ_I were found to increase compared to the other locations.

IV. Experimental Analysis of Co-Channel Interference and Background Noise in BANs

In this section, we begin by developing a theoretical expression for the outage probability (OP) of κ-μ fading channels which are subject to CCI and BN. We then utilize the parameter estimates obtained in Section III to provide some useful insights into the performance of BANs that are subject to CCI and BN, as well as making some important recommendations on the thresholds which must be maintained to ensure adequate outage performance.

The OP of the signal-to-interference-plus-noise-ratio (SINR) is defined as the probability that the instantaneous SINR falls below a given threshold, γ_{th}; that is

$$P_{\text{OP}}(\gamma_{\text{th}}) = \mathbb{P}\left(\frac{P_S|h_S|^2}{P_I|h_I|^2 + N_0} \leq \gamma_{\text{th}}\right) = \mathbb{P}(\gamma_S \leq (\gamma_I + 1)\gamma_{\text{th}}) \quad (2)$$

where $|h_S|$ and $|h_I|$ represent the envelope of the channel fading coefficient for the SoI and the interfering channels, respectively; and P_S, P_I, and N_0 denote the transmit power at the source of the SoI, the transmit power of the interferer's signal and the noise power at the intended receiver, respectively. The instantaneous SNR of the SoI is then given by $\gamma_S = ((P_S|h_S|^2)/N_0)$, while the instantaneous interference-to-noise-ratio (INR) is given by $\gamma_I = ((P_I|h_I|^2)/N_0)$.

A theoretical expression for the OP over κ-μ/κ-μ[3] fading channels in an interference limited scenario with restricted values of the μ parameter was presented in [18]. This was later extended to include arbitrary μ parameters in [19]. However, neither study was able to obtain closed-form expressions that included BN which is also known to affect the performance of wireless systems. As demonstrated in Section III, the estimates of κ and μ for both the on-body SoI and the inter-BAN interference channels are non-identical. Furthermore, the μ estimates are less than unity and therefore non-integers. Hence, it is necessary to formulate an expression for the OP over κ-μ fading channels in the presence of CCI and BN for independent and non-identically distributed ($i.n.i.d$) κ-μ variates, without parameter constraints.

In [20], it was shown that computing the OP of a system with CCI and BN is equivalent to calculating its secrecy outage probability (SOP) when the interferer is replaced with an eavesdropper. Capital-

[3]It should be noted that κ-μ/κ-μ indicates that the SoI and the interferer are both subject to κ-μ fading.

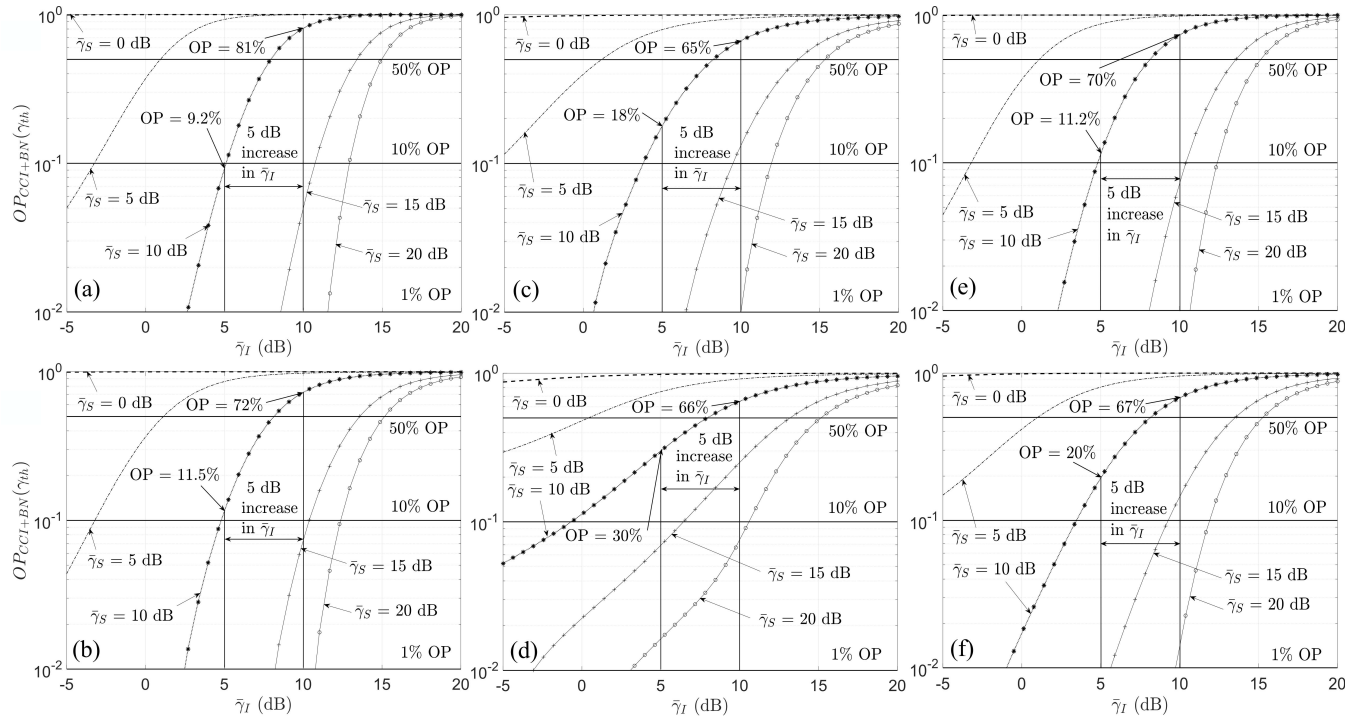

Fig. 5. OP with CCI + BN for increasing values of $\bar{\gamma}_S$ versus $\bar{\gamma}_I$ in the anechoic chamber for (a) scenario 1 and (b) scenario 2; reverberation chamber for (c) scenario 1 and (d) scenario 2; and laboratory environment for (e) scenario 1 and (f) scenario 2. $\gamma_{\text{th}} = 1.5$ dB and $\bar{\gamma}_S = 0$, 5, 10, 15, and 20 dB.

izing on this observation [20, Table 1], along with the SOP results presented in [19], we establish the theoretical OP of κ-μ fading channels which are subject to *i.n.i.d* fading. Making the following substitutions: $\gamma_{\text{thS}} \to \gamma_{\text{th}}$, where γ_{thS} is the secrecy threshold SNR, $\gamma_E \to \gamma_I(\gamma_{\text{th}}/(1+\gamma_{\text{th}}))$, $\gamma_M \to \gamma_S$, $\{\kappa_M, \mu_M\} \to \{\kappa_S, \mu_S\}$ and $\{\kappa_E, \mu_E\} \to \{\kappa_I, \mu_I\}$ in [19, eq. 14] along with some mathematical manipulations, the OP of the SINR of κ-μ fading channels is

$$P_{\text{OP}}(\gamma_{\text{th}}) = 1 - \frac{\mu_I(1+\kappa_I)^{\frac{\mu_I+1}{2}}}{\kappa_I^{\frac{\mu_I-1}{2}} \bar{\gamma}_I^{\frac{\mu_I+1}{2}} e^{\mu_I\kappa_I}} \int_0^{\infty} \gamma_I^{\frac{\mu_I-1}{2}} \times e^{\frac{-\mu_I(1+\kappa_I)\gamma_I}{\bar{\gamma}_I}} I_{\mu_I-1}\left(2\mu_I\sqrt{\frac{\kappa_I(1+\kappa_I)\gamma_I}{\bar{\gamma}_I}}\right) \times Q_{\mu_S}\left(\sqrt{2\kappa_S\mu_S}, \sqrt{\frac{2(1+\kappa_S)\gamma_{\text{th}}(1+\gamma_I)\mu_S}{\bar{\gamma}_S}}\right) d\gamma_I \tag{3}$$

where $\bar{\gamma}_S$ and $\bar{\gamma}_I$ denote the average SNR and the average INR at the intended receiver, respectively. Unfortunately at present, it is not possible to obtain a closed form solution to (3) because of its complicated integral representation. Nonetheless, this was not the objective of the study performed here, rather to gain important insights into the performance of BANs subject to CCI and BN using channel measurements. Hence, the ensuing analysis will be performed with respect to (3) in conjunction with the parameter estimates obtained in Section III. For each of the environments and scenarios, we evaluate the performance of the BAN system when $\gamma_{\text{th}} = 1.5$ dB, $\bar{\gamma}_S$ is fixed at 10 dB and for three different levels of P_{OP}, namely, 0.01 (1% OP level), 0.1 (10% OP level), and 0.5 (50% OP level). These are indicative of very low, relatively low, and mid-range levels of outage probabilities, respectively. Nonetheless, it should be noted that the experimental results (parameter estimates) and the theoretical expressions provided mean that the interested reader can evaluate the BAN system performance for their chosen values of γ_{th}, $\bar{\gamma}_S$, $\bar{\gamma}_I$, and the necessary OP.

A. Anechoic Chamber

Using the parameter estimates given in Table I, Fig. 5(a) and (b) depicts the estimated OP versus $\bar{\gamma}_I$ during scenarios 1 and 2, respectively. As annotated in Fig. 5(a), when $\bar{\gamma}_S = 10$ dB it can be observed that if $\bar{\gamma}_I$ is increased from 5 to 10 dB, the OP of the BAN system will increase from 9.2% to 81%. This severe degradation in the channel's quality is due to the increased interference introduced by the inter-BAN interferer. For this scenario, to ensure a very low, relatively low or mid-range OP level of 1%, 10%, or 50% for the SoI link, $\bar{\gamma}_I$ must not exceed 2.6, 5.1, and 7.9 dB, respectively.

Considering the same procedure for scenario 2 with $\bar{\gamma}_S = 10$ dB [Fig. 5(b)], we find that an increase in $\bar{\gamma}_I$ from 5 to 10 dB significantly degrades the quality of the SoI channel. This is evidenced by the increase in the OP, which rises from 11.5% to 72%. Additionally, we observe that $\bar{\gamma}_I$ should not be greater than 2.4, 4.8, and 8.1 dB to ensure very low, relatively low, or mid-range OP levels of 1%, 10%, or 50% for the SoI channel, respectively.

B. Reverberation Chamber

Fig. 5(c) shows the OP of the BAN system versus $\bar{\gamma}_I$ for scenario 1. With $\bar{\gamma}_S$ fixed at 10 dB, we observe that increasing $\bar{\gamma}_I$ from 5 to 10 dB causes the OP of the BAN system to rise from 18% to 65%. This increase in the OP was found to be lower than that observed for scenario 1 in the anechoic chamber. Moreover, to ensure low OP levels of 1% or 10% for the SoI link, we find that $\bar{\gamma}_I$ must not exceed 0.7 and 3.8 dB, respectively. Likewise, to ensure a mid-range OP level of 50% for the SoI, $\bar{\gamma}_I$ must not exceed 8.2 dB.

From Fig. 5(d), with $\bar{\gamma}_S = 10$ dB, we see that if $\bar{\gamma}_I$ is increased from 5 to 10 dB the OP increases from 30% to 66%. As well as this, for this fading environment we observe that $\bar{\gamma}_I$ should not be greater

than -5, -0.5, and 7.9 dB to ensure low and mid-range OP levels of 1%, 10%, or 50% for the SoI channel, respectively.

C. Laboratory Environment

From Fig. 5(e), we find that for scenario 1 (as with the previous two environments), if $\bar{\gamma}_I$ improves from 5 to 10 dB, the OP of the BAN system increases from 11.2% to 70%. To ensure low and mid-range OP levels of 1%, 10%, or 50% for the SoI link, $\bar{\gamma}_I$ should not surpass 2.3, 4.8, and 8 dB respectively.

For scenario 2 [see Fig. 5(f)], increasing $\bar{\gamma}_I$ from 5 to 10 dB causes an increase in the OP of the BAN system from 20% to 67%. Furthermore, the average SNR of the interferer must not exceed -0.9, 3.5, and 8.2 dB to ensure low and midrange OP levels of 1%, 10%, and 50% for the SoI.

V. Conclusion

In this communication, we have performed a systematic investigation of the performance of BAN channels which are subject to κ-μ fading in the presence of CCI and BN. Considering three environments with differing multipath intensities it was observed that the κ and μ parameter estimates for the SoI were greater than those obtained for the interfering link. Furthermore, the estimates of κ were found to decrease while the μ parameter estimates were found to increase, as both the BAN user and the interferer moved from anechoic to scenarios with environmental multipath. Utilizing the empirical characterization of the short-term fading in BANs, we investigated the OP of BAN communications in which the SoI and the interference channels experience κ-μ fading. Our results have provided important insights into the outage performance of BANs which are subject to CCI and BN. Most notably, the performance of the BAN system in the low multipath environments was found to be worse when compared to more reverberant environments. Furthermore, a higher OP was observed when both persons (i.e., the BAN user and interferer) were mobile compared to the scenario when only one person was moving.

References

[1] A. Alomainy *et al.*, "Statistical analysis and performance evaluation for on-body radio propagation with microstrip patch antennas," *IEEE Trans. Antennas Propag.*, vol. 55, no. 1, pp. 245–248, Jan. 2007.

[2] P. S. Hall *et al.*, "Antennas and propagation for on-body communication systems," *IEEE Antennas Propag. Mag.*, vol. 49, no. 3, pp. 41–58, Jun. 2007.

[3] S. L. Cotton and W. G. Scanlon, "An experimental investigation into the influence of user state and environment on fading characteristics in wireless body area networks at 2.45 GHz," *IEEE Trans. Wireless Commun.*, vol. 8, no. 1, pp. 6–12, Jan. 2009.

[4] A. Fort, C. Desset, P. De Doncker, P. Wambacq, and L. Van Biesen, "An ultra-wideband body area propagation channel Model-from statistics to implementation," *IEEE Trans. Microw. Theory Techn.*, vol. 54, no. 4, pp. 1820–1826, Jun. 2006.

[5] S. L. Cotton and W. G. Scanlon, "Channel characterization for single- and multiple-antenna wearable systems used for indoor body-to-body communications," *IEEE Trans. Antennas Propag.*, vol. 57, no. 4, pp. 980–990, Apr. 2009.

[6] S. L. Cotton, W. G. Scanlon, and J. Guy, "The $\kappa-\mu$ distribution applied to the analysis of fading in body to body communication channels for fire and rescue personnel," *IEEE Antennas Wireless Propag. Lett.*, vol. 7, pp. 66–69, 2008.

[7] R. Rosini, R. Verdone, and R. D'Errico, "Body-to-body indoor channel modeling at 2.45 GHz," *IEEE Trans. Antennas Propag.*, vol. 62, no. 11, pp. 5807–5819, Nov. 2014.

[8] Z. H. Hu, Y. Nechayev, and P. Hall, "Measurements and statistical analysis of the transmission channel between two wireless body area networks at 2.45GHz and 5.8GHz," in *Proc. IEEE ICECom*, Sep. 2010, pp. 1–4.

[9] Y. Wang, I. B. Bonev, J. Ø. Nielsen, I. Z. Kovacs, and G. F. Pedersen, "Characterization of the indoor multiantenna body-to-body radio channel," *IEEE Trans. Antennas Propag.*, vol. 57, no. 4, pp. 972–979, Apr. 2009.

[10] M. D. Yacoub, "The κ-μ distribution and the η-μ distribution," *IEEE Antennas Propag. Mag.*, vol. 49, no. 1, pp. 68–81, Feb. 2007.

[11] L. Hanlen, D. Miniutti, D. Smith, D. Rodda, and B. Gilbert, "Co-channel interference in body area networks with indoor measurements at 2.4 GHz: Distance-to-interferer is a poor estimate of received interference power," *Int. J. Wireless Inf. Netw.*, vol. 17, nos. 3–4, pp. 113–125, 2010.

[12] X. Wu, Y. I. Nechayev, C. C. Constantinou, and P. S. Hall, "Interuser interference in adjacent wireless body area networks," *IEEE Trans. Antennas Propag.*, vol. 63, no. 10, pp. 4496–4504, Oct. 2015.

[13] B. de Silva, A. Natarajan, and M. Motani, "Inter-user interference in body sensor networks: Preliminary investigation and an infrastructure-based solution," in *Proc. 6th Int. Workshop Wearable Implant. Body Sensor Netw.*, Berkeley, CA, USA, Jun. 2009, pp. 35–40.

[14] I. Khan, P. S. Hall, Y. I. Nechayev, and L. Akhoondzadeh-Asl, "Multiple antenna systems for increasing on-body channel capacity and reducing BAN-to-BAN interference," in *Proc. IEEE Int. Workshop Antenna Technol. (iWAT)*, Mar. 2010, pp. 1–4.

[15] R. de Francisco, L. Huang, and G. Dolmans, "Coexistence of WBAN and WLAN in medical environments," in *Proc. IEEE 70th Veh. Technol. Conf. Fall*, Anchorage, AK, USA, Sep. 2009, pp. 1–5.

[16] G. A. Conway and W. G. Scanlon, "Antennas for over-body-surface communication at 2.45 GHz," *IEEE Trans. Antennas Propag.*, vol. 57, no. 4, pp. 844–855, Apr. 2009.

[17] T. S. Rappaport, *Wireless Communications: Principles and Practice*, vol. 2. Upper Saddle River, NJ, USA: Prentice-Hall, 1996.

[18] N. Y. Ermolova and O. Tirkkonen, "Laplace transform of product of generalized Marcum Q, Bessel I, and power functions with applications," *IEEE Trans. Signal Process.*, vol. 62, no. 11, pp. 2938–2944, Jun. 2014.

[19] N. Bhargav, S. L. Cotton, and D. E. Simmons, "Secrecy capacity analysis over κ-μ fading channels: Theory and applications," *IEEE Trans. Commun.*, vol. 64, no. 7, pp. 3011–3024, Jul. 2016.

[20] G. Gomez, F. J. Lopez-Martinez, D. Morales-Jimenez, and M. R. McKay, "On the equivalence between interference and eavesdropping in wireless communications," *IEEE Trans. Veh. Technol.*, vol. 64, no. 12, pp. 5935–5940, Dec. 2015.